

# SPHinXsys: an open-source multi-physics and multi-resolution library based on smoothed particle hydrodynamics

Chi Zhang<sup>a</sup>, Massoud Rezavand<sup>a</sup>, Yujie Zhu<sup>a</sup>, Yongchuan Yu<sup>b</sup>, Dong Wu<sup>a</sup>, Wenbin Zhang<sup>a</sup>, Jianhang Wang<sup>a</sup>, Xiangyu Hu<sup>a,\*</sup>

<sup>a</sup>*Department of Mechanical Engineering, Technical University of Munich, 85748 Garching, Germany*

<sup>b</sup>*Department of Aerospace and Geodesy, Technical University of Munich, 82024 Taufkirchen, Germany*

---

## Abstract

In this paper, we present an open-source multi-resolution and multi-physics library: SPHinXsys (pronunciation: s'finksis) which is an acronym for Smoothed Particle Hydrodynamics (SPH) for industrial compleX systems. As an open-source library, SPHinXsys is developed and released under the terms of Apache License (2.0). Along with the source code, a complete documentation is also distributed to make the compilation and execution easy. SPHinXsys aims at modeling coupled multi-physics industrial dynamic systems including fluids, solids, multi-body dynamics and beyond, in a multi-resolution unified SPH framework. As an SPH solver, SPHinXsys has many advantages namely, (1) the generic design provides a C++ API showing a very good flexibility when building domain-specific applications, (2) numerous industrial or scientific applications can be coupled within the same framework and (3) with the open-source philosophy, the community of users can collaborate and improve the library. SPHinXsys presently (v0.2.0) includes validations and applications in the fields of fluid dynamics, solid dynamics, thermal and mass diffusion, reaction-diffusion, electromechanics and fluid-structure interactions (FSI).

*Keywords:* Open-source library, Smoothed Particle Hydrodynamics, Meshless method, Multi-physics solver, Multi-resolution solver

---

## PROGRAM SUMMARY

*Program Title:* SPHinXsys

*Current Version:* v0.2.0

*CPC Library link to program files:* (to be added by Technical Editor)

*Repository link:* <https://github.com/Xiangyu-Hu/SPHinXsys>

*Code Ocean capsule:* <https://doi.org/10.24433/CO.0560985.v1>

*Licensing provisions:* Apache-2.0

*Programming language:* C++

*Dependencies:* cmake, Boost, Threading Building Blocks (TBB), SimBody

*Computing platforms:* Linux, Mac OS, Microsoft Windows

*Support email:* c.zhang@tum.de, xiangyu.hu@tum.de

## 1. Introduction

As an open-source multi-resolution and multi-physics library based on the smoothed particle hydrodynamics (SPH) method, SPHinXsys has been developed for modeling the industrial complex systems in the following fields: fluid dynamics, solid mechanics, fluid-structure interaction (FSI), thermal and mass diffusion, reaction diffusion, electromechanics and the beyond.

---

\*Corresponding author.

*Email addresses:* c.zhang@tum.de (Chi Zhang), massoud.rezavand@tum.de (Massoud Rezavand), yujie.zhu@tum.de (Yujie Zhu), yongchuan.yu@tum.de (Yongchuan Yu), dong.wu@tum.de (Dong Wu), wenbin.zhang@tum.de (Wenbin Zhang), jianhang.wang@tum.de (Jianhang Wang), xiangyu.hu@tum.de (Xiangyu Hu)

The main numerical development features of SPHinXsys v0.2.0 are listed below:

- low-dissipation SPH method base on Riemann solvers for violent free-surface flow involving breaking and impact [1];
- dual-criteria time stepping method for weakly compressible SPH (WCSPH) method[2];
- multi-resolution SPH method for fluid-structure interaction (FSI) [3];
- position-based Verlet time stepping scheme [3];
- schemes for thermal and mass iso- and anisotropic diffusion [4];
- schemes for reaction-diffusion models [4];
- schemes for electromechanics [4];

SPHinXsys is based on SPH, for unified modeling of fluid dynamics, thermal and mass diffusion, reaction diffusion and their coupling with solid mechanics. SPH method is a fully Lagrangian particle based method, in which the continuum media is discretized into Lagrangian particles and the mechanics is approximated as the interaction between them using a kernel function, usually a Gaussian-like function. As a meshless method, SPH does not require a mesh to define the neighboring interaction configuration of particles, however, the construction and updated configurations according to the distance between particles is essential. A remarkable feature of this method is that its computational algorithm involves a large number of common abstractions, i.e. particles, which are suitable to inherently cope with many physical systems. Due to such unique features, SPHinXsys has intrinsic advantages for modeling multi-physics systems. The theory and fundamentals of the SPH method are briefly summarized in Section 1.1

This paper is structured as follows. The main numerical schemes of SPHinXsys dealing with fluid dynamics are summarized in Section 2, solid mechanics in Section 3, thermal and mass diffusion in Section 4, reaction-diffusion models in Section 5, FSI problems in Section 6, position-based Verlet time stepping algorithm in Section 7 and with the electromechanics in Section 8. Furthermore, the source code and the executables are presented

in Section 9. The code validations and applications are next summarized in Section 10 and finally, the concluding remarks and future works are noted in Section 11.

### 1.1. Theory and fundamentals of SPH

In the SPH method, a variable field  $f(\mathbf{r})$  in a continuum medium is discretized as a particle system

$$f_i = \int f(\mathbf{r})W(\mathbf{r}_i - \mathbf{r}, h)d\mathbf{r}. \quad (1)$$

Here,  $i$  is the particle index,  $f_i$  the discretized particle-average variable and  $\mathbf{r}_i$  the particle position. The compact-support kernel function  $W(\mathbf{r}_i - \mathbf{r}, h)$ , where  $h$  is the smoothing length, is radially symmetric with respect to  $\mathbf{r}_i$ . Since we assume that the mass of each particle  $m_i$  is known and invariant (indicating mass conservation), one has the particle volume  $V_i = m_i/\rho_i$ , where  $\rho_i$  is the particle-average density.

In SPH, a variable can be approximated by the particle-average values

$$f(\mathbf{r}) \approx \sum_j V_j W(\mathbf{r} - \mathbf{r}_j, h) f_j = \sum_j \frac{m_j}{\rho_j} W(\mathbf{r} - \mathbf{r}_j, h), \quad (2)$$

where the summation is over all the neighboring particles  $j$  located in the support domain of the particle of interest, and leads to an approximation of the particle-average density

$$\rho_i \approx \sum_j m_j W(\mathbf{r}_i - \mathbf{r}_j, h) = \sum_j m_j W_{ij}, \quad (3)$$

which is an alternative way to the continuity equation for updating the fluid density.

The dynamics of other particle-average variables is based on a general form of interaction between a particle and its neighbors, i.e. the approximation of the spatial derivative operators on the right hand sides (RHS) of the evolution equations. The original SPH approximation of the derivative of a variable field  $f(\mathbf{r})$  at particle  $i$  is obtained by the following formulation

$$\begin{aligned} \nabla f_i &\approx \int_{\Omega} \nabla f(\mathbf{r})W(\mathbf{r}_i - \mathbf{r}, h)dV \\ &= - \int_{\Omega} f(\mathbf{r})\nabla W(\mathbf{r}_i - \mathbf{r}, h)dV \approx - \sum_j V_j \nabla_i W_{ij} f_j. \end{aligned} \quad (4)$$

Here,  $\nabla_i W_{ij} = \mathbf{e}_{ij} \frac{\partial W_{ij}}{\partial r_{ij}}$  with  $r_{ij}$  and  $\mathbf{e}_{ij}$  are the distance and unit vector of the particle pair  $(i, j)$ , respectively.

Note that, Eq. (4) can be modified into a strong form

$$\nabla f_i = f_i \nabla 1 + \nabla f_i \approx \sum_j V_j \nabla_i W_{ij} f_{ij}, \quad (5)$$

where  $f_{ij} = f_i - f_j$  is the inter-particle difference value. The strong-form approximation of the derivative is used to determine the local structure of a field. Also, with a slight different modification, Eq. (4) can be rewritten into a weak form as

$$\nabla f_i = \nabla f_i - f_i \nabla 1 \approx -2 \sum_j V_j \nabla W_{ij} \tilde{f}_{ij}, \quad (6)$$

where  $\tilde{f}_{ij} = (f_i + f_j)/2$  is the inter-particle average value. The weak-form approximation of derivative is used to compute the surface integration respected to a variable for solving its conservation law. Due to the anti-symmetric property of the derivative of the kernel function, i.e.  $\nabla_i W_{ij} = -\nabla_j W_{ji}$ , it implies the momentum conservation of the particle system.

Since its invention by Lucy [5] and Gingold and Monaghan [6] for modeling astrophysics problems, SPH has been successfully exploited in a broad variety of problems ranging from fluid dynamics [7, 8, 9, 10] to solid mechanics [11, 12, 13, 14], fluid-structure interactions (FSI) [15, 16, 3], and multi-phase flows [17].

## 2. Schemes for fluid dynamics

### 2.1. Governing equation

In the Lagrangian frame, the conservation of mass and momentum for fluid dynamics can be written as

$$\begin{cases} \frac{d\rho}{dt} = -\rho \nabla \cdot \mathbf{v} \\ \rho \frac{d\mathbf{v}}{dt} = -\nabla p + \eta \nabla^2 \mathbf{v} + \rho \mathbf{g} \end{cases}, \quad (7)$$

where  $\mathbf{v}$  is the velocity,  $\rho$  the density,  $p$  the pressure,  $\eta$  the dynamic viscosity,  $\mathbf{g}$  the gravity and  $\frac{d}{dt} = \frac{\partial}{\partial t} + \mathbf{v} \cdot \nabla$  stands for material derivative. For modeling incompressible flow with weakly compressible assumption [7, 18], an artificial isothermal equation of state (EoS) is introduced to close Eq. (7)

$$p = c^2(\rho - \rho^0). \quad (8)$$

With the weakly compressible assumption, the density varies around 1% [18] if an artificial sound speed of  $c = 10U_{max}$  is employed, with  $U_{max}$  being the maximum anticipated flow speed.

### 2.2. WCSPH method based on Riemann solvers

In SPHinXsys, the WCSPH method based on Riemann solvers is applied for fluid dynamics, where the continuity and momentum equations are discretized as [1, 2]

$$\begin{cases} \frac{d\rho_i}{dt} = 2\rho_i \sum_j \frac{m_j}{\rho_j} (U^* - \mathbf{v}_i \cdot \mathbf{e}_{ij}) \frac{\partial W_{ij}}{\partial r_{ij}} \\ \frac{d\mathbf{v}_i}{dt} = -2 \sum_j m_j \frac{P^*}{\rho_i \rho_j} \nabla_i W_{ij} \end{cases}. \quad (9)$$

Here,  $U^*$  and  $P^*$  are the solutions of inter-particle Riemann problem along the unit vector  $\mathbf{e}_{ij} = -\mathbf{r}_{ij}/r_{ij}$  pointing from particle  $i$  to  $j$ . SPHinXsys applies a low-dissipation Riemann solver [1].

For viscous flows, the physical shear term can be discretized as [8]

$$\left(\frac{d\mathbf{v}_i}{dt}\right)^{(v)} = 2 \sum_j m_j \frac{\eta}{\rho_i \rho_j} \frac{\mathbf{v}_{ij}}{r_{ij}} \frac{\partial W_{ij}}{\partial r_{ij}}, \quad (10)$$

where  $\eta$  is the dynamic viscosity.

For high Reynolds number flows, the WCSPH method may suffer from tensile instability which induces particle clumping or void region. To remedy this issue, we apply the transport velocity formulation [19, 20]

$$\frac{d\bar{\mathbf{v}}_i}{dt} = \frac{d\mathbf{v}_i}{dt} - 2 \sum_j m_j \frac{p^0}{\rho_i \rho_j} \nabla_i W_{ij}, \quad (11)$$

for modeling flows without free surface. Here,  $p^0$  is the background pressure and  $\bar{\mathbf{v}}$  represents the particle transport velocity.

In SPHinXsys, a density initialization scheme is introduced to stabilize the density which is updated by continuity equation in Eq. 9. At the beginning of the new step, the fluid density field of free-surface flows is reinitialized by

$$\rho_i = \max(\rho^*, \rho^0 \frac{\sum W_{ij}}{\sum W_{ij}^0}), \quad (12)$$

where  $\rho^*$  denotes the density before re-initialization and superscript 0 represents the initial reference value. For flows without free surface, Eq. 12 is merely modified as

$$\rho_i = \rho^0 \frac{\sum W_{ij}}{\sum W_{ij}^0}. \quad (13)$$

### 2.3. Wall boundary condition

In the WCSPH method explained in 2.2, the interaction between fluid particles and wall particles is determined by solving a one-sided Riemann problem [1] along the wall normal direction.

In the one-sided Riemann problem the left state is defined from the fluid particle corresponding to the local boundary normal,

$$(\rho_L, U_L, P_L) = (\rho_f, -\mathbf{n}_w \cdot \mathbf{v}_f, P_f) \quad (14)$$

where the subscript  $f$  represents the fluid particles and  $\mathbf{n}_w$  the local wall normal direction. According to the physical wall boundary condition the right state velocity  $U_R$  is assumed as

$$U_R = -U_L + 2u_w, \quad (15)$$

where  $u_w$  is the wall velocity. Similar to Adami et al. [21] the right state pressure is assumed as

$$P_R = P_L + \rho_f \mathbf{g} \cdot \mathbf{r}_{fw}, \quad (16)$$

where  $\mathbf{r}_{fw} = \mathbf{r}_w - \mathbf{r}_f$ , and the right state density is obtained by applying the artificial equation of state.

### 2.4. Dual-criteria time stepping

SPHinXsys applies the dual-criteria time stepping for the integration of fluid equation. Following Ref. [2], two time-step size criteria, viz. the advection criterion termed  $\Delta t_{ad}$  is defined as

$$\Delta t_{ad} = CFL_{ad} \min\left(\frac{h}{|\mathbf{v}|_{max}}, \frac{h^2}{\nu}\right), \quad (17)$$

and the acoustic criterion termed  $\Delta t_{ac}$  is given by

$$\Delta t_{ac} = CFL_{ac} \frac{h}{c + |\mathbf{v}|_{max}}. \quad (18)$$

Here,  $CFL_{ad} = 0.25$ ,  $CFL_{ac} = 0.6$ , and  $|\mathbf{v}|_{max}$  is the maximum particle advection velocity in the flow while  $\nu$  denotes the kinematic viscosity. Accordingly, the advection criterion controls the updating frequency of particle configuration and the acoustic criterion determines the frequency of the pressure relaxation process.

## 3. Schemes for solid dynamics

### 3.1. Kinematics and governing equation

The kinematics of the finite deformations can be characterized by introducing a deformation map  $\varphi$ , which maps a material point  $\mathbf{r}^0$  from the initial reference configuration  $\Omega^0 \subset \mathbb{R}^d$  to the point  $\mathbf{r} = \varphi(\mathbf{r}^0, t)$  in the deformed configuration  $\Omega = \varphi(\Omega^0)$ . Here, the superscript  $(\bullet)^0$  denotes the quantities in the initial reference configuration. Then, the deformation tensor  $\mathbb{F}$  can be defined by its derivative with respect to the initial reference configuration as

$$\mathbb{F} = \nabla^0 \varphi = \frac{\partial \varphi}{\partial \mathbf{r}^0} = \frac{\partial \mathbf{r}}{\partial \mathbf{r}^0}. \quad (19)$$

Also, the deformation tensor  $\mathbb{F}$  can be calculated from the displacement  $\mathbf{u} = \mathbf{r} - \mathbf{r}^0$  through

$$\mathbb{F} = \nabla^0 \mathbf{u} + \mathbb{I}, \quad (20)$$

where  $\mathbb{I}$  represents the unit matrix. For incompressible material, we have the constraint

$$J = \det(\mathbb{F}) \equiv 1. \quad (21)$$

Associated with  $\mathbb{F}$  are the right and left Cauchy-Green deformation tensors defined by

$$\mathbb{C} = \mathbb{F}^T \cdot \mathbb{F} \quad \text{and} \quad \mathbb{B} = \mathbb{F} \cdot \mathbb{F}^T, \quad (22)$$

respectively. Then, four typical invariants of  $\mathbb{C}$  (and also of  $\mathbb{B}$ ) can be defined as

$$\begin{aligned} I_I &= \text{tr}(\mathbb{C}), & I_{ff} &= \mathbf{f}^0 \cdot (\mathbb{C}\mathbf{f}^0), \\ I_{ss} &= \mathbf{s}^0 \cdot (\mathbb{C}\mathbf{s}^0), & I_{fs} &= \mathbf{f}^0 \cdot (\mathbb{C}\mathbf{s}^0), \end{aligned} \quad (23)$$

where  $\mathbf{f}^0$  and  $\mathbf{s}^0$  are the non-deformed myocardial fiber and sheet unit direction, respectively. Here,  $I_I$  is the first principal invariant,  $I_{ff}$  and  $I_{ss}$  are the structure based invariants and  $I_{fs}$  is the fiber-sheet shear [22].

In a Lagrangian framework, the conservation of mass and the linear momentum corresponding to the cardiac mechanics can be expressed as

$$\begin{cases} \rho = \rho_0 \frac{1}{J} \\ \rho^0 \frac{d\mathbf{y}}{dt} = \nabla^0 \cdot \mathbb{P}^T + \rho^0 \mathbf{g} \end{cases} \quad \Omega^0 \times [0, T], \quad (24)$$

where  $\rho$  is the density and  $\mathbb{P}$  the first Piola-Kirchhoff stress tensor and  $\mathbb{P} = \mathbb{F}\mathbb{S}$  with  $\mathbb{S}$  denoting the second Piola-Kirchhoff stress tensor. In particular, when the material is linear elastic and isotropic, the constitutive equation is simply given by

$$\begin{aligned}\mathbb{S} &= K \operatorname{tr}(\mathbb{E}) \mathbb{I} + 2G \left( \mathbb{E} - \frac{1}{3} \operatorname{tr}(\mathbb{E}) \mathbb{I} \right) \\ &= \lambda \operatorname{tr}(\mathbb{E}) \mathbb{I} + 2\mu \mathbb{E},\end{aligned}\quad (25)$$

where  $\lambda$  and  $\mu$  are Lamé parameters,  $K = \lambda + (2\mu/3)$  the bulk modulus and  $G = \mu$  the shear modulus. The relation between the two modulus is given by

$$E = 2G(1 + 2\nu) = 3K(1 - 2\nu) \quad (26)$$

with  $E$  denoting the Young's modulus and  $\nu$  the Poisson ratio. Note that the sound speed of solid structure is defined as  $c^S = \sqrt{K/\rho}$ . The Neo-Hookean material model can be defined in general form by the strain-energy density function

$$W = \mu \operatorname{tr}(\mathbb{E}) - \mu \ln J + \frac{\lambda}{2} (\ln J)^2. \quad (27)$$

Note that the second Piola-Kirchhoff stress  $\mathbb{S}$  can be derived as

$$\mathbb{S} = \frac{\partial W}{\partial \mathbb{E}} \quad (28)$$

from strain-energy density function.

### 3.2. Total Lagrangian formulation

For solid mechanics, SPHinXsys applies the total Lagrangian formulation where the initial reference configuration is used for finding the neighboring particles and the set of neighboring particles is not altered.

Firstly, a correction matrix  $\mathbb{B}^0$  [23] is introduced as

$$\mathbb{B}_i^0 = \left( \sum_j V_j (\mathbf{r}_j^0 - \mathbf{r}_i^0) \otimes \nabla_i^0 W_{ij} \right)^{-1}, \quad (29)$$

where

$$\nabla_i^0 W_{ij} = \frac{\partial W(\|\mathbf{r}_{ij}^0\|, h)}{\partial \|\mathbf{r}_{ij}^0\|} \mathbf{e}_{ij}^0 \quad (30)$$

denotes the gradient of the kernel function evaluated at the initial reference configuration. It is worth noting that

the correction matrix is computed in the initial configuration and therefore, it is calculated only once before the simulation. Then, the momentum conservation equation, Eq.(24), can be discretized as

$$\begin{cases} \rho_i = \rho_0 \frac{1}{\det(\mathbb{F})} \\ \frac{d\mathbf{v}_i}{dt} = \frac{2}{m_i} \sum_j V_j V_j \tilde{\mathbb{P}}_{ij} \nabla_i^0 W_{ij} + \mathbf{g} \end{cases}, \quad (31)$$

where the inter-particle averaged first Piola-Kirchhoff stress  $\tilde{\mathbb{P}}$  is defined as

$$\tilde{\mathbb{P}}_{ij} = \frac{1}{2} (\mathbb{P}_i \mathbb{B}_i^0 + \mathbb{P}_j \mathbb{B}_j^0). \quad (32)$$

Note that the first Piola-Kirchhoff stress tensor is computed from the constitutive law with the deformation tensor  $\mathbb{F}$  is given by

$$\mathbb{F} = \left( \sum_j V_j (\mathbf{u}_j - \mathbf{u}_i) \otimes \nabla_i^0 W_{ij} \right) \mathbb{B}_i^0 + \mathbb{I}. \quad (33)$$

## 4. Schemes for thermal and mass diffusion

### 4.1. Governing equation

Thermal or mass diffusion, in particular anisotropic diffusion, occurs in many physical applications, e.g. thermal conduction in fusion plasma, image processing, biological processes and medical imaging. The governing equations for thermal or mass diffusion reads

$$\frac{dC}{dt} = \nabla \cdot (\mathbb{D} \nabla C), \quad (34)$$

where  $C$  is the concentration of a compound and  $\mathbb{D}$  is the diffusion coefficient in iso- and aniso-tropic forms.

### 4.2. SPH discretization for the anisotropic diffusion equation

In SPHinXsys, the diffusion equation is discretized by an anisotropic SPH discretization scheme modified from the work of Tran-Duc et al. [24]. Following Ref. [24], the diffusion tensor  $\mathbb{D}$  is considered to be a symmetric positive-definite matrix and can be decomposed by Cholesky decomposition as

$$\mathbb{D} = \mathbb{L}\mathbb{L}^T \quad (35)$$

where  $\mathbb{L}$  is a lower triangular matrix with real and positive diagonal entries and  $\mathbb{L}^T$  denotes the transpose of  $\mathbb{L}$ . Eq. (46) can be rewritten in isotropic form as

$$\nabla \cdot (\mathbb{D}\nabla) = \nabla \cdot (\mathbb{L}\mathbb{L}^T\nabla) = (\mathbb{L}^T\nabla)^T \cdot (\mathbb{L}^T\nabla) = \widetilde{\nabla}^2, \quad (36)$$

where  $\widetilde{\nabla} = \mathbb{L}^T\nabla$ . Then, the new isotropic diffusion operator is approximated by the following kernel integral by neglecting the high-order term

$$\widetilde{\nabla} \cdot (\widetilde{\nabla})C = 2 \int_{\Omega} \frac{C(\widetilde{\mathbf{r}}) - C(\widetilde{\mathbf{r}'})}{|\widetilde{\mathbf{r}} - \widetilde{\mathbf{r}}'|} \frac{\partial W(\widetilde{\mathbf{r}} - \widetilde{\mathbf{r}}', \widetilde{h})}{\partial |\widetilde{\mathbf{r}} - \widetilde{\mathbf{r}}'|} d\widetilde{\mathbf{r}}, \quad (37)$$

where  $\widetilde{\mathbf{r}} = \mathbb{L}^{-1}\mathbf{r}$  and  $\widetilde{h} = \mathbb{L}^{-1}h$ . Upon the coordinate transformation, the kernel gradient can be rewritten as

$$\frac{\partial W(\widetilde{\mathbf{r}} - \widetilde{\mathbf{r}}', \widetilde{h})}{\partial (\widetilde{\mathbf{r}} - \widetilde{\mathbf{r}}')} = \frac{1}{\|\mathbb{L}^{-1}\| \|\mathbb{L}^{-1}\mathbf{e}_{\widetilde{\mathbf{r}\mathbf{r}}}\|} \frac{\partial W(\mathbf{r} - \mathbf{r}')}{\partial |\mathbf{r} - \mathbf{r}'|} \quad (38)$$

with  $\mathbf{e}_{\mathbf{r}\mathbf{r}} = \frac{\mathbf{r}' - \mathbf{r}}{|\mathbf{r}' - \mathbf{r}|}$ . Finally, Eq. (36) can be discretized in SPH form as

$$\widetilde{\nabla}^2 C \approx 2 \sum_j^N \frac{m_j}{\rho_j} \left( C(\mathbf{r}_i) - C(\mathbf{r}_j) \right) \frac{1}{(\widetilde{\mathbb{L}}_{ij}\mathbf{e}_{ij})^2} \frac{1}{r_{ij}} \frac{\partial W_{ij}}{\partial r_{ij}}, \quad (39)$$

by replacing the term  $\mathbb{L}_{ij}^{-1}$  with its linear approximation  $\widetilde{\mathbb{L}}_{ij}$  given by

$$\widetilde{\mathbb{L}}_{ij} = \frac{\widetilde{\mathbb{L}}_i \widetilde{\mathbb{L}}_j}{\widetilde{\mathbb{L}}_i + \widetilde{\mathbb{L}}_j} \quad (40)$$

where  $\widetilde{\mathbb{L}}_i$  is defined as

$$\widetilde{\mathbb{D}}_i = (\widetilde{\mathbb{L}}_i^{-1}) (\widetilde{\mathbb{L}}_i^{-1})^T. \quad (41)$$

In this case, the Cholesky decomposition and the corresponding matrix inverse are computed once for each particle before the simulation. Also, Eq. (39) can be rewritten by introducing a kernel correction matrix Eq. (29) as

$$\frac{dC}{dt} = 2 \sum_j \frac{m_j}{\rho_j} \left( \mathbb{B}_i^0 C(\mathbf{r}_i) - \mathbb{B}_j^0 C(\mathbf{r}_j) \right) \cdot \frac{\mathbf{e}_{ij} \cdot \mathbf{e}_{ij}}{(\widetilde{\mathbb{L}}_{ij}\mathbf{e}_{ij})^2} \frac{1}{r_{ij}} \frac{\partial W_{ij}}{\partial r_{ij}}. \quad (42)$$

## 5. Schemes for reaction-diffusion model

### 5.1. Governing equation

In recent years, the reaction-diffusion model has attracted a considerable deal of attention due to its ubiquitous application in many fields of science. The reaction-diffusion model can generate a wide variety of spatial patterns, which has been widely applied in chemistry, biology, and physics, even used to explain self-regulated pattern formation in the developing animal embryo. The general form of reaction-diffusion model reads

$$\frac{dV}{dt} = \nabla \cdot (\mathbb{D}\nabla V) + I(V), \quad (43)$$

where  $\mathbb{D}$  is diffusion tensor and  $I(V)$  a nonlinear function. For  $I(V) = V - V^3$ , Eq. (43) becomes the Allen-Cahn equation, which describes the mixture of two incompressible fluids. When the FitzHugh-Nagumo model [25] is applied, Eq. (43) becomes the well known mono domain equation [26] which describes the cell electrophysiological dynamics. Electrophysiological dynamics of the heart describe how electrical currents flow through the heart, controlling its contractions, and are used to ascertain the effects of certain drugs designed to treat, for example, arrhythmia.

The Fitzhugh-Nagumo (FN) model reads [25]

$$\begin{cases} I(V, w) = -V(V - a)(V - 1) - w \\ \dot{w} = g(V, w) = \epsilon_0(\beta V - \gamma w - \sigma) \end{cases}, \quad (44)$$

where  $\epsilon_0$ ,  $\beta$ ,  $\gamma$  and  $\sigma$  are suitable constant parameters, given specifically.

The Aliev-Panfilov (AP) model [27], a variant of the FN model, has been successfully implemented in the simulations of ventricular fibrillation in real heart geometries [28] and it is particularly suitable for the problems where electrical activity of the heart is of the main interest. The AP model has the following form

$$\begin{cases} I(V, w) = -kV(V - a)(V - 1) - wV \\ \dot{w} = g(V, w) = \epsilon(V, w)(-kV(V - b - 1) - w) \end{cases}, \quad (45)$$

where  $\epsilon(V, w) = \epsilon_0 + \mu_1 w / (\mu_2 + V_m)$  and  $k$ ,  $a$ ,  $b$ ,  $\epsilon_0$ ,  $\mu_1$  and  $\mu_2$  are suitable constant parameters.

### 5.2. SPH method for reaction-diffusion

The reaction-diffusion model consists of a coupled system of partial differential equations (PDE) governing the diffusion process as well as ordinary differential equations (ODE) governing the reactive kinetics of the gating variable. In SPHinXsys, the operator splitting method [26] is applied and results in a PDE governing the anisotropic diffusion

$$\frac{dV}{dt} = \nabla \cdot (\mathbb{D} \nabla V), \quad (46)$$

and two ODEs

$$\begin{cases} \frac{dV}{dt} = I(V, w) \\ \frac{dw}{dt} = g(V, w) \end{cases}, \quad (47)$$

where  $I(V, w)$  and  $g(V, w)$  are defined by the FN model Eq. (44) or the AP model Eq. (45). The schemes for discretizing the diffusion equation is presented in Section 4.

### 5.3. Reaction-by-reaction splitting

In SPHinXsys, a reaction-by-reaction splitting method [29] is introduced for solving the system of ODEs defined by Eq. (47), which is generally stiff and induces numerical instability when the integration time step is not sufficiently small. The multi-reaction system can be decoupled using the second-order accurate Strang splitting as

$$R^{(\Delta t)} = R_V^{(\frac{\Delta t}{2})} \circ R_w^{(\frac{\Delta t}{2})} \circ R_w^{(\frac{\Delta t}{2})} \circ R_V^{(\frac{\Delta t}{2})}, \quad (48)$$

where the  $\circ$  symbol separates each reaction and indicates that the operator  $R_V^{(\Delta t)}$  is applied after  $R_w^{(\Delta t)}$ . Note that the reaction-by-reaction splitting methodology can be extended to more complex ionic models, e.g. the Tusscher-Panfilov model [30].

Following Ref. [29], we rewrite the Eq. (47) in the following form

$$\frac{dy}{dt} = q(y, t) - p(y, t)y, \quad (49)$$

where  $q(y, t)$  is the production rate and  $p(y, t)y$  is the loss rate [29]. The general form of Eq. (49), where the analytical solution is not explicitly known or difficult to derive, can be solved by using the quasi steady state (QSS) method for an approximate solution as

$$y^{n+1} = y^n e^{-p(y^n, t)\Delta t} + \frac{q(y^n, t)}{p(y^n, t)} (1 - e^{-p(y^n, t)\Delta t}). \quad (50)$$

Note that the QSS method is unconditionally stable due to the analytic form, and thus a larger time step is allowed for the splitting method, leading to a higher computational efficiency.

## 6. Multi-resolution FSI coupling

SPHinXsys benefits from a multi-resolution framework, i.e. the fluid and solid equations are discretized by different spatial-temporal resolutions, for modeling FSI problems. More precisely, different particle spacing, hence different smoothing lengths, and different time steps are utilized to discretize the fluid and solid equations [3].

In the multi-resolution framework, the governing equations of Eq. (7) are discretized as

$$\begin{cases} \frac{d\rho_i}{dt} = 2\rho_i \sum_j \frac{m_j}{\rho_j} (U^* - \mathbf{v}_i \cdot \mathbf{e}_{ij}) \frac{\partial W_{ij}^{h^F}}{\partial r_{ij}} \\ \frac{d\mathbf{v}_i}{dt} = -2 \sum_j m_j \frac{p^*}{\rho_i \rho_j} \nabla_i W_{ij}^{h^F} + \mathbf{g} + \mathbf{f}_i^{S:p}(h^F) + \mathbf{f}_i^{S:v}(h^F) \end{cases}, \quad (51)$$

where  $h^F$  represents the smoothing length used for fluid.

Also, the discretization of solid equation of Eq. (31) is modified to

$$\begin{cases} \rho_a = \rho_0 \frac{1}{\det(\mathbb{F})} \\ \frac{d\mathbf{v}_a}{dt} = \frac{2}{m_a} \sum_b V_b \tilde{\mathbb{P}}_{ab} \nabla_a^0 W_{ab} + \mathbf{g} + \mathbf{f}_a^{F:p}(h^F) + \mathbf{f}_a^{F:v}(h^F) \end{cases}, \quad (52)$$

where  $h^S$  denotes the smoothing length used for solid discretization. Generally, we use  $h^F$  assuming  $h^F \geq h^S$ . In more details, the forces  $\mathbf{f}_i^{S:p}(h^F)$  and  $\mathbf{f}_i^{S:v}(h^F)$  of Eq. (51) are modified to

$$\mathbf{f}_i^{S:p}(h^F) = -2 \sum_a V_i V_a \frac{p_i \rho_a^d + p_a^d \rho_i}{\rho_i + \rho_a^d} \nabla_i W(\mathbf{r}_{ia}, h^F) \quad (53)$$

and

$$\mathbf{f}_i^{S:v}(h^F) = 2 \sum_a \eta V_i V_a \frac{\mathbf{v}_i - \mathbf{v}_a^d}{|\mathbf{r}_{ia}| + 0.01h} \frac{\partial W(\mathbf{r}_{ia}, h^F)}{\partial r_{ia}}. \quad (54)$$

The fluid forces exerting on the solid structure  $\mathbf{f}_a^{F:p}(h^F)$  and  $\mathbf{f}_a^{F:v}(h^F)$  are straightforward to derive.

The multi time stepping scheme for FSI is coupled with the dual-criteria time stepping presented in Section 2.4. More precisely, during each fluid acoustic time step (Eq.

(18)) the structure time integration  $\kappa = \lceil \frac{\Delta t^F}{\Delta t^S} \rceil + 1$  marches with the solid time-step criterion

$$\Delta t^S = 0.6 \min \left( \frac{h^S}{c^S + |\mathbf{v}|_{max}}, \sqrt{\frac{h^S}{|\frac{d\mathbf{v}}{dt}|_{max}}} \right). \quad (55)$$

As different time steps are applied in the integration of fluid and solid equations, we redefine the imaginary pressure  $p_a^d$  and velocity  $\mathbf{v}_a^d$  in Eqs. (53) and (54) as

$$\begin{cases} p_a^d = p_i + \rho_i \max(0, (\mathbf{g} - \frac{d\widetilde{\mathbf{v}}_a}{dt}) \cdot \mathbf{n}^S)(\mathbf{r}_{ia} \cdot \mathbf{n}^S) \\ \mathbf{v}_a^d = 2\mathbf{v}_i - \widetilde{\mathbf{v}}_a \end{cases}, \quad (56)$$

where (56)  $\widetilde{\mathbf{v}}_a$  and  $\frac{d\widetilde{\mathbf{v}}_a}{dt}$  represent the single averaged velocity and acceleration of solid particles during a fluid acoustic time step.

## 7. Position-based Verlet scheme

SPHinXsys applies the position-based Verlet scheme for the time integration of fluid and solid equation. As presented in Ref. [3], the position-based Verlet achieves strict momentum conservation in fluid-structure coupling when multiple time steps is employed. In the position-based Verlet scheme, a half step for position is followed by a full step for velocity and another half step for position. Denoting the values at the beginning of a fluid acoustic time step by superscript  $n$ , at the mid-point by  $n + \frac{1}{2}$  and eventually at the end of the time-step by  $n + 1$ , here we summarize the scheme. At first, the integration of the fluid is conducted as

$$\begin{cases} \rho_i^{n+\frac{1}{2}} = \rho_i^n + \frac{1}{2} \Delta t_{ac}^F \frac{d\rho_i}{dt} \\ \mathbf{r}_i^{n+\frac{1}{2}} = \mathbf{r}_i^n + \frac{1}{2} \Delta t_{ac}^F \mathbf{v}_i^n \end{cases}, \quad (57)$$

by updating the density and position fields into the mid-point. The particle velocity is next updated to the new time step in the following form

$$\mathbf{v}_i^{n+1} = \mathbf{v}_i^n + \Delta t_{ac}^F \frac{d\mathbf{v}_i}{dt}. \quad (58)$$

Finally, the position and density of fluid particles are updated to the new time step by

$$\begin{cases} \mathbf{r}_i^{n+1} = \mathbf{r}_i^{n+\frac{1}{2}} + \frac{1}{2} \Delta t_{ac}^F \mathbf{v}_i \\ \rho_i^{n+1} = \rho_i^{n+\frac{1}{2}} + \frac{1}{2} \Delta t_{ac}^F \frac{d\rho_i}{dt} \end{cases}. \quad (59)$$

For solid equations, index  $\varkappa = 0, 1, \dots, \kappa - 1$  is used to denote integration step for solid particles. With the position-based Verlet scheme, the deformation tensor, density and particle position are updated to the midpoint as

$$\begin{cases} \mathbb{F}_a^{\varkappa+\frac{1}{2}} = \mathbb{F}_a^{\varkappa} + \frac{1}{2} \Delta t^S \frac{d\mathbb{F}_a}{dt} \\ \rho_a^{\varkappa+\frac{1}{2}} = \rho_a^0 \frac{1}{J} \\ \mathbf{r}_a^{\varkappa+\frac{1}{2}} = \mathbf{r}_a^{\varkappa} + \frac{1}{2} \Delta t^S \mathbf{v}_a \end{cases}. \quad (60)$$

The velocity is next updated by

$$\mathbf{v}_a^{\varkappa+1} = \mathbf{v}_a^{\varkappa} + \Delta t^S \frac{d\mathbf{v}_a}{dt}. \quad (61)$$

Lastly, the deformation tensor and position of solid particles are updated to the new time step of the solid structure with

$$\begin{cases} \mathbb{F}_a^{\varkappa+1} = \mathbb{F}_a^{\varkappa+\frac{1}{2}} + \frac{1}{2} \Delta t^S \frac{d\mathbb{F}_a}{dt} \\ \rho_a^{\varkappa+1} = \rho_a^0 \frac{1}{J} \\ \mathbf{r}_a^{\varkappa+1} = \mathbf{r}_a^{\varkappa+\frac{1}{2}} + \frac{1}{2} \Delta t^S \mathbf{v}_a^{\varkappa+1} \end{cases}. \quad (62)$$

## 8. Electromechanics

As the multi-physics modeling of the complete cardiac process, including the muscle tissues, is one of the main future goals of SPHinXsys, the active stress approach is applied for modeling the electromechanics. Following the work of Nash and Panfilov [31], the stress tensor is coupled with the transmembrane potential  $V_m$  through the active stress approach, which decomposes the first Piola-Kirchhoff stress  $\mathbb{P}$  into passive and active parts

$$\mathbb{P} = \mathbb{P}_{passive} + \mathbb{P}_{active}. \quad (63)$$

Here, the passive component  $\mathbb{P}_{passive}$  describes the stress required to obtain a given deformation of the passive myocardium, and an active component  $\mathbb{P}_{active}$  denotes the tension generated by the depolarization of the propagating transmembrane potential.

For the passive mechanical response, we consider the Holzapfel-Odgen model, which proposed the following strain energy function, considering different contributions and taking the anisotropic nature of the myocardium into account. To ensure that the stress vanishes in the reference

configuration and encompasses the finite extensibility, we modify the strain-energy function as

$$\begin{aligned} \mathbf{W} &= \frac{a}{2b} \exp[b(I_1 - 3)] - a \ln J + \frac{\lambda}{2} (\ln J)^2 \\ &+ \sum_{i=f,s} \frac{a_i}{2b_i} \{\exp[b_i(I_{ii} - 1)^2] - 1\} \\ &+ \frac{a_{fs}}{2b_{fs}} \{\exp[b_{fs}I_{fs}^2] - 1\}, \end{aligned} \quad (64)$$

where  $a$ ,  $b$ ,  $a_f$ ,  $b_f$ ,  $a_s$ ,  $b_s$ ,  $a_{fs}$  and  $b_{fs}$  are eight positive material constants, with the  $a$  parameters having the dimension of stress and  $b$  parameters being dimensionless. Here, the second Piola-Kirchhoff stress  $\mathbb{S}$  is defined by

$$\mathbb{S} = 2 \frac{\partial \mathbf{W}}{\partial \mathbf{C}} - p \mathbf{C}^{-1} = 2 \sum_j \frac{\partial \mathbf{W}}{\partial I_j} \frac{\partial I_j}{\partial \mathbf{C}} - p \mathbf{C}^{-1} \quad (65)$$

$j = I, ff, ss, fs,$

where

$$\frac{\partial I_1}{\partial \mathbf{C}} = \mathbb{I}, \quad \frac{\partial I_{ff}}{\partial \mathbf{C}} = \mathbf{f}_0 \otimes \mathbf{f}_0, \quad (66)$$

$$\frac{\partial I_{ss}}{\partial \mathbf{C}} = \mathbf{f}_0 \otimes \mathbf{f}_0, \quad \frac{\partial I_{fs}}{\partial \mathbf{C}} = \mathbf{f}_0 \otimes \mathbf{s}_0 + \mathbf{s}_0 \otimes \mathbf{f}_0, \quad (67)$$

and  $p$  is the Lagrange multiplier arising from the imposition of incompressibility. Substituting Eqs. (65) and (66) into Eq.(64) the second Piola-Kirchhoff stress is given as

$$\begin{aligned} \mathbb{S} &= a \exp[b(I_1 - 3)] + \{\lambda \ln J - a\} \mathbf{C}^{-1} \\ &+ 2a_f (I_f - 1) \exp[b_f (I_f - 1)^2] \mathbf{f}_0 \otimes \mathbf{f}_0 \\ &+ 2a_s (I_s - 1) \exp[b_s (I_s - 1)^2] \mathbf{s}_0 \otimes \mathbf{s}_0 \\ &+ a_{fs} I_{fs} \exp[b_{fs} (I_{fs})^2] \mathbf{f}_0 \otimes \mathbf{f}_0. \end{aligned} \quad (68)$$

Following the active stress approach proposed by Nash and Panfilov [31], the active component provides the internal active contraction stress by

$$\mathbb{P}_{active} = T_a \mathbb{F} \mathbf{f}_0 \otimes \mathbf{f}_0, \quad (69)$$

where  $T_a$  represents the active magnitude of the stress and its evolution is given by an ODE as

$$\dot{T}_a = \epsilon(V_m) [k_a (V_m - V_r) - T_a], \quad (70)$$

where parameters  $k_a$  and  $V_r$  control the maximum active force, the resting action potential and the activation function [32]

$$\epsilon(V_m) = \epsilon_0 + (\epsilon_\infty - \epsilon_{-\infty}) \exp\{-\exp[-\xi(V_m - \bar{V}_m)]\}. \quad (71)$$

Here, the limiting values  $\epsilon_{-\infty}$  at  $V_m \rightarrow -\infty$  and  $\epsilon_\infty$  at  $V_m \rightarrow \infty$ , the phase shift  $\bar{V}_m$  and the transition slope  $\xi$  will ensure a smooth activation of the muscle traction.

## 9. Source code

In this section, an overview of SPHinXsys is given in Section 9.1, a synthetic description of the program units is reported in Section 9.2 and a brief summary of the installation instructions is given in Section 9.3. For more details, the readers are referred to the documentation presented in SPHinXsys's repository.

### 9.1. Overview

In SPHinXsys, the whole computational domain is modeled as SPH bodies and each body is composed of an ensemble of SPH particles. See Figure 9.1 for a typical example in the simulation of flow induced vibration of a flexible beam attached to a rigid cylinder. Note that a SPH solid body may be composed of more than one components. As shown in Fig. 9.1, while the wall body has two rigid solid components, the solid obstacle is composed of a rigid and an elastic component. The particle interaction is decomposed into two parts: 1) inner interaction, which represents the interaction of two neighboring particles located in the same SPH body; and 2) contact interaction, which denotes the interaction of two neighboring particles originated from different SPH bodies.

### 9.2. Synthetic description of the program units

Folders of SPHinXsys repository are reported in Table 9.1. The program units of SPHinXsys v0.2.0 (folder "SPHinXsys") are grouped in subfolders, associated with the following topics: data structure and general functions for vector and scalar data (Table 9.2); SPHBody and the derived FluidBody and SolidBody (Table 9.3); geometry representation of SPHBody (Table 9.4); material property (Table 9.5); Kernel function (Table 9.6); meshes for level-set and cell-linked lists (Table 9.7); particle container (Table 9.8); particle generator (Table 9.9); particle dynamics

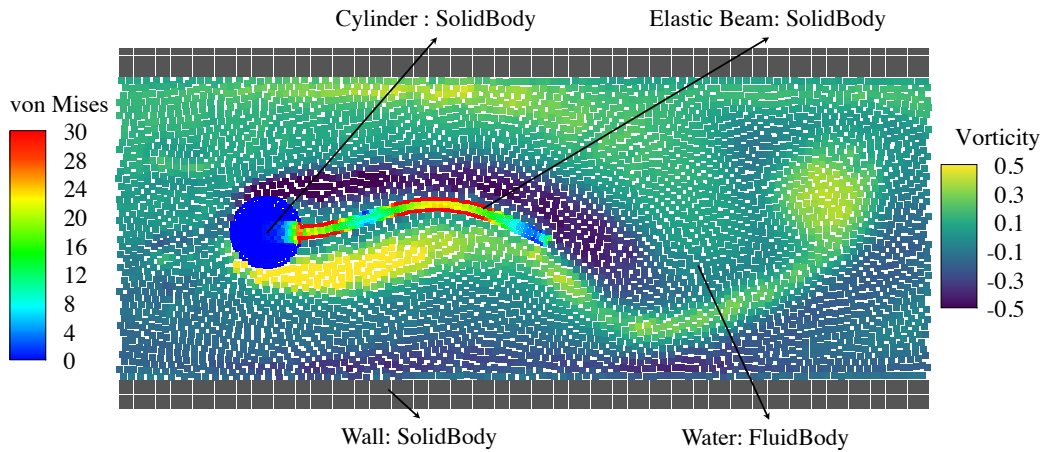


Figure 9.1: A typical FSI problem involving a rigid solid (wall) body, a composite solid (obstacle) body and a fluid body. The wall body has two (upper and lower) components. The obstacle body is composed of a rigid (cylinder) and an elastic (beam) components.

(Table 9.10); interface for Simbody (Table 9.11) and in-and output system (“I/O”, Table 9.12).

The optional input files of SPHinXsys are listed here:

- ensemble of points and their volumes for generating particles directly
- ensemble of points in 2D for representing polygon
- ploymesh in STL or OBJ format for representing 3D geometry

The main output files of SPHinXsys report the following information:

- basic parameters for test cases
- particle data in PLT or VTU formats for different visualization methods
- time series of the observed variables for the monitoring probes

### 9.3. Installation and execution

SPHinXsys source and executable files are distributed on a dedicated Git repository on GitHub. The executable files are released for cross-platform building, including Linux, MAC OSX and Microsoft Windows. SPHinXsys depends on the following libraries:

- cross-platform building: cmake 3.14.0 or later.
- compiler: Visual Studio 2017 or later (Windows only), gcc 4.9 or later (typically on Linux), or Apple Clang (1001.0.46.3) or later
- BOOST library (newest version)
- TBB library (newest version)
- Simbody library 3.6.0 or later
- linear algebra: LAPACK 3.5.0 or later and BLAS

The general procedure for installing and executing SPHinXsys is as follows:

- installing the dependencies and set up the system variables in your machine as shown in Table 9.13
- download the source code or clone the git repository
- create a directory in which the user will build a SPHinXsys project, e.g. ”/simbody-build”
- configure the SPHinXsys build with CMake
- compile and run the tests

For more details, the readers are referred to the repository page <https://github.com/Xiangyu-Hu/SPHinXsys>

Table 9.1: Folders of SPHinXsys v0.2.0 repository.

| Folder              | Description  |
|---------------------|--|
| (repository folder) | Readme, installation instruction, Doxyfile and Apache license file |
| doc                 | Documentation file   |
| cmake               | cmake files for multi-platform compilation and dependencies search |
| cases_test          | Executable code for test cases                                     |
| SPHinXsys           | Source code for the CPU compilation                                |

Table 9.2: Program units (".h" and ".cpp") for the basic data types in folder "SPHinXsys/src/share/base\_data.type".

| Program unit         | Description   |
|----------------------|---|
| large_data_container | Definition of vector and matrix data structures                           |
| scalar_functions     | Functions for scalar data, e.g., ABS, AMAX, AMIN and SGN                  |
| small_vectors        | Functions for vector data, e.g. sorting, shuffle, difference and subtract |

Table 9.3: Program units (".h" and ".cpp") for the SPHBody in folder "SPHinXsys/src/share/bodies".

| Program unit  | Description  |
|---------------|--|
| base_body     | Base class of SPHBody                                      |
| fluid_body    | Fluid-like SPHBody which contains fluid property           |
| solid_body    | Solid-like SPHBody which contains solid property           |
| body_relation | Relationship, inner or contact interaction, between bodies |

Table 9.4: Program units (".h" and ".cpp") for the geometry representation in folder "SPHinXsys/src/share/base\_geometry".

| Program unit  | Description  |
|---------------|--|
| base_geometry | Base class of geometry   |
| geometry      | Geometry representation of SPHBody<br>2D geometry is based on polygon provided by Boost library<br>3D geometry is based on parsing polymesh in STL or OBJ format |

Table 9.5: Program units (".h" and ".cpp") for the Kernel in folder "SPHinXsys/src/share/kernels".

| Program unit      | Description                   |
|-------------------|-------------------------------|
| base_kernel       | Base class of Kernel function |
| kernel_hyperbolic | Hyperbolic kernel [33]        |
| kernel_wenland_c2 | Wenland C2 kernel [34]        |

Table 9.6: Program units (".h" and ".cpp") for material in folder "SPHinXsys/src/share/materials".

| Program unit              | Description                               |
|---------------------------|---|
| base_material             | Base class of material                    |
| weakly_compressible_fluid | Fluid with weakly-compressible assumption |
| elastic_solid             | Elastic solid                             |
| diffusion_reaction        | Reaction-diffusion model                  |

Table 9.7: Program units (".h" and ".cpp") for the mesh in folder "SPHinxsys/src/share/meshes".

| Program unit          | Description                                       |
|-----------------------|---|
| base_mesh             | Base class of Mesh and the derived level-set mesh |
| mesh_cell_linked_list | Background mesh for cell-linked lists             |

Table 9.8: Program units (".h" and ".cpp") for the particle in folder "SPHinxsys/src/share/particles".

| Program unit                 | Description  |
|------------------------------|--|
| base_particles               | Class of BaseParticles which contains position, velocity and volume data         |
| fluid_particles              | Particles which contains fluid properties, e.g. density, mass and pressure       |
| solid_particles              | Particles which contains elastic solid properties, e.g. density, mass and stress |
| diffusion_reaction_particles | Particles which contains diffusion-reaction properties, e.g. species             |
| neighbor_relation            | Particle interaction configuration, including kernel value and the gradients     |

Table 9.9: Program units (".h" and ".cpp") for the particle generator in folder "SPHinxsys/src/share/particle\_generator".

| Program unit               | Description   |
|----------------------------|---|
| base_particle_generator    | Base class of particle generator                                  |
| particle_generator_lattice | Particle direct generator by reading particle position and volume |
| particle_generator_lattice | Particle generator on Lattice point                               |

## 10. Validations and applications

SPHinxsys has been validated and applied on more than 20 test cases, whose main program are updated with the last code release. Some of them are briefly described in the following and also referred to the corresponding publications. The aim of this section is to recall the code validations and applications. The references for details and validations on the single test cases are available in the following subsections, which are grouped according to the associated fields: fluid dynamics (Section 10.1), solid mechanics (Section 10.2), FSI (Section 10.3), thermal and mass diffusion (Section 10.4, reaction-diffusion (Section 10.5) and electromechanics (Section 10.6).

### 10.1. Fluid dynamics

In the context of modeling fluid dynamic, the WCSPH method is widely applied for the simulation of violent free-surface flows exhibiting violent events such as impact and breaking. Typical examples include dambreak flow, sloshing and wave impact, as well as fluid-solid interactions. Here, four benchmark tests involving violent free-surface flow are briefly summarized to validate SPHinxsys.

The first two tests, viz. 2D and 3D dambreak flows (folders "cases\_test/test\_2d\_dambreak" and "cases\_test/test\_3d\_dambreak"), allow us to quantitatively validate the program against the available experimental data. Figure 10.1a and 10.1b illustrate the snapshots of the free surface with the main features, including high roll-up along the downstream wall and a large reflected jet, being well captured. The third example simulates a dambreak flow interacting with a fixed obstacle and the solid boundaries of the domain as shown in Figure 10.1c. As another challenging problem, 3D sloshing tank has also been validated in SPHinxsys, which is introductory to the fuel/liquid natural gas (LNG) sloshing tank applications. Figure 10.1d shows the particle and pressure distributions when a high run-up forms and impacts to the wall. For all the test cases, validation of the time history of impact pressure is documented by comparing the numerical results with the experimental data [2].

### 10.2. Solid dynamics

SPHinxsys has been validated on preliminary benchmarks in 2D and 3D for solid dynamics where structure experiences large deformation.

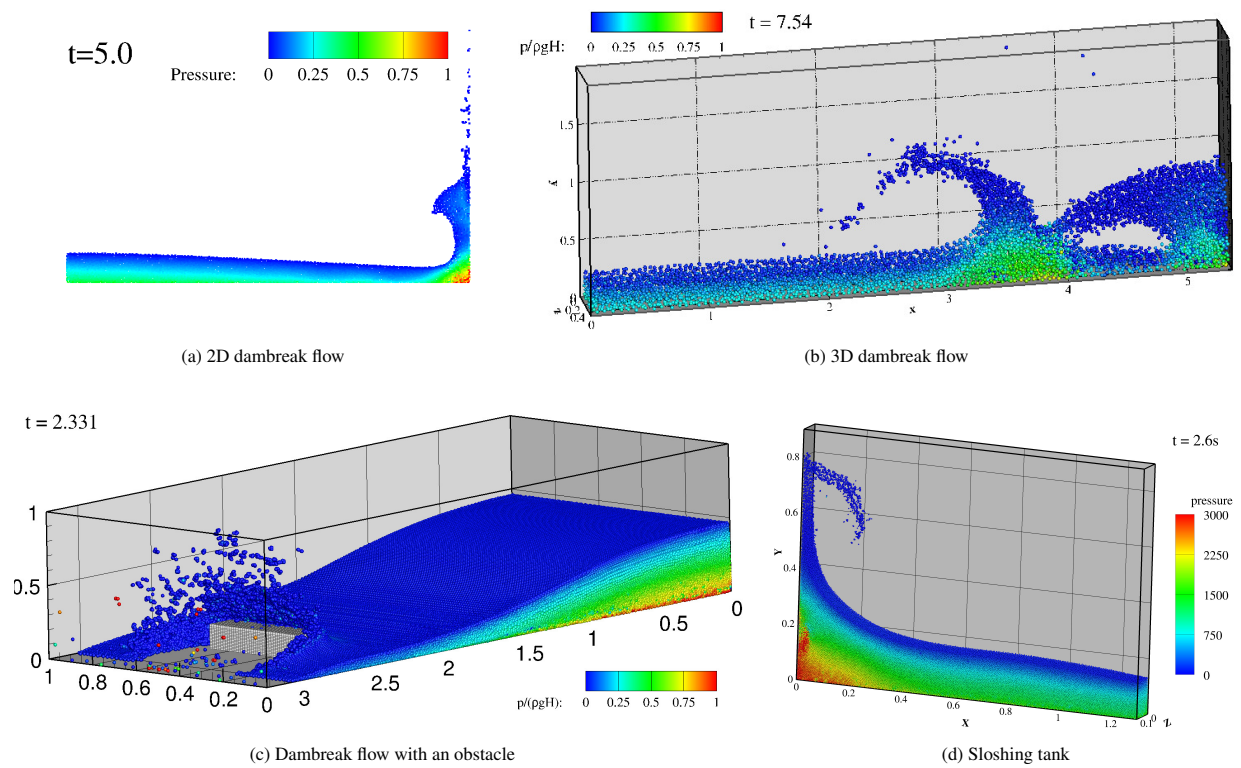


Figure 10.1: SPHinXsys validations and applications for free-surface flows with violent wave-breaking and impact events. (a) Two-dimensional dambreak flow. (b) Three-dimensional dambreak flow. (c) Three-dimensional dambreak flow impact on a obstacle. (d) Sloshing tank under resonance .

Table 9.10: Program units (".h", ".hpp" and ".cpp") for the particle dynamics in folder "SPHinxsys/src/share/particle\_dynamics".

| Program unit   | Description  |
|--|--|
| base_particle_dynamics   | Base classes of particle dynamics describing the particle interaction which defines differential operators for fluxes in continuum mechanics   |
| particle_dynamics_algorithms   | Particle dynamics describe 3 types of particle interaction:<br>1) Simple dynamics for updating particle state without particle-interaction<br>2) Inner dynamics for inner particle-interaction<br>3) Complex dynamics for inner and contact particle-interactions  |
| external_force<br>subfolder "./external_force"                           | Apply the gravity or body force to momentum equation   |
| general_dynamics<br>subfolder "./general_dynamics"                       | Particle dynamics for applying periodic, in- and outflow BCs, implementing ghost-particle BCs and randomized particle position   |
| fluid_dynamics<br>subfolder "./fluid_dynamics"                           | Fluid particle dynamics for:<br>1) Setting up the initial condition<br>2) Computing advection and acoustic timestep size<br>3) Computing particle number density<br>4) Applying transport-velocity formulation<br>5) Calculating viscous force<br>6) Implementing the density initialization algorithm.<br>7) Integrating momentum equation with position-based Verlet scheme  |
| solid_dynamics<br>subfolder "./solid_dynamics"                           | Solid particle dynamics for :<br>1) Setting up the initial condition<br>2) Computing acoustic timestep size<br>3) Computing or updating the normal direction of structure<br>4) Computing the kernel correction matrix<br>5) Computing pressure and viscous force form the fluid<br>6) Integrating momentum equation with position-based Verlet scheme<br>7) Computing total force on solid body for Simbody integration<br>8) Constrain particle in solid body from Simbody integration state |
| diffusion_reaction_dynamics<br>subfolder "./diffusion_reaction_dynamics" | Particle dynamics for :<br>1) Integrating the diffusion process with RK2 scheme<br>2) Integrating the reaction process with RBR splitting method   |
| active_muscle_dynamics<br>subfolder "./active_muscle_dynamics"           | Computing electro-mechanical feedback  |

Table 9.11: Program units (".h" and ".cpp") for the interface with Simbody in folder "SPHinxsys/src/share/simbody".

| Program unit | Description   |
|--------------|---|
| state_engine | Interface for parsing state of MobilizedBody in Simbody |
| xml_engine   | Interface for XML data parsing                          |

The first benchmark, 2D oscillating beam (folder "cases\_test/test\_2d\_oscillating\_beam") where a thin elastic beam initially stimulated by a velocity profile with one end fixed and another free, is investigated to demonstrate the numerical accuracy of solid mechanics solver in SPHinxsys. Figure 10.2a shows the particle and von

Table 9.12: Program units (".h" and ".cpp") for the I/O system in folder "SPHinxsys/src/share/io\_system".

| Program unit | Description  |
|--------------|--|
| in_output    | Particle data read and write in XML format for restart       |
|              | Particle data output in PLT and VTU format for visualization |
|              | Observed data output in DAT format for formal analysis       |

Table 9.13: System variables for dependencies search.

| System variables | Path                                |
|------------------|-------------------------------------|
| TBB_HOME         | path/to/TBB-installation-prefix     |
| BOOST_HOME       | path/to/boost-installation-prefix   |
| SIMBODY_HOME     | path/to/Simbody-installation-prefix |

Mises stress distribution when the beam reaches its maximum deformation. This test allows evaluating the accuracy for solid dynamics and code validation can be attained through the analytical solution. In the second test, cantilever bending (folder "cases\_test/test\_3d\_cantilever") where a 3D rubber-like cantilever, whose bottom face is clamped to the ground and its body is allowed to bend freely by imposing an initial uniform velocity, is considered. Figure 10.2b shows the deformed configuration colored with von Mises stress and for the quantitative comparison with data in literature the reader is referred to Ref. [4].

### 10.3. Fluid-structure interactions

In this part, three benchmark FSI tests, viz. a hydrostatic water column on an elastic plate, a flow-induced vibration and a dambreak flow with elastic gate, are studied in multi-resolution scenarios to validate the FSI solvers in SPHinxsys.

In the first test, plate deformation under hydrostatic pressure of a water column is considered. Figure 10.3a gives the time histories of the mid-span displacement, together with the convergence study with increasing spatial resolution of structure while the resolutions of fluid is constant. A high-order convergence of the middle-span displacement is observed. In the second benchmark (folder "cases\_test/test\_2d\_fsi"), a two dimensional flow-induced vibration of a flexible beam attached to a rigid cylinder is studied. Figure 10.3b shows the flow vorticity field and beam deformation when self-sustained oscillation is reached. Furthermore, we consider the deforma-

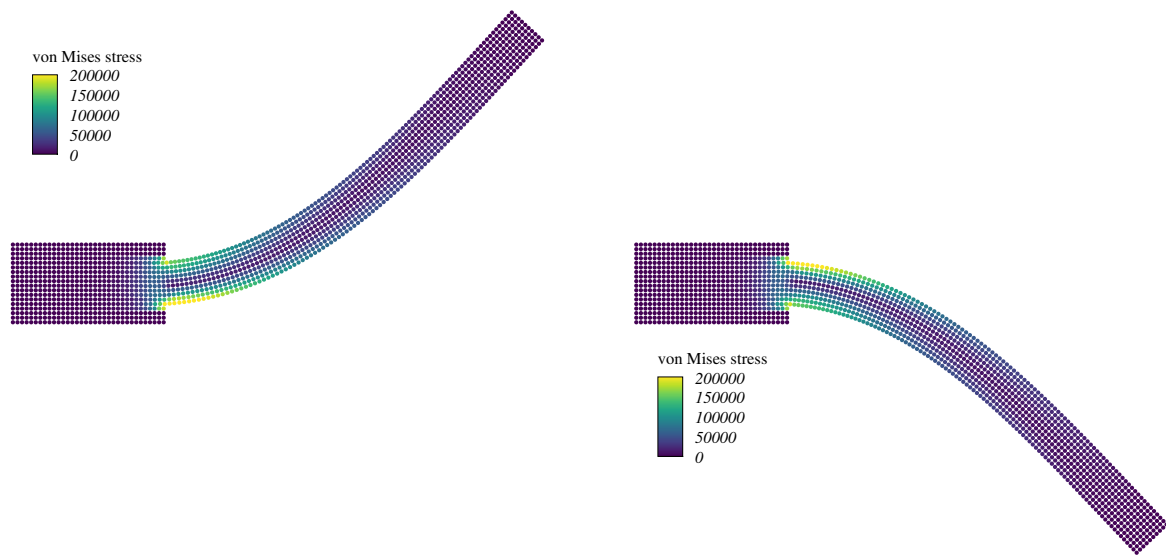
tion of an elastic plate subjected to a time-dependent water pressure (folder "cases\_test/test\_2d\_dambreak\_gate"). The comparison between the numerical snapshots and the experiment presented by Antoci et al. [15] is illustrated in Figure 10.3c. It can be observed that the simulation results are in a good agreement with the experimental results.

Concerning the computational efficiency, with the multi-resolution treatments of SPHinxsys up to 240 and 960 times speed ups are achieved when the fluid-structure resolution ratio is 2 and 4, respectively. These computational efficiency analysis are carried out for the first benchmark.

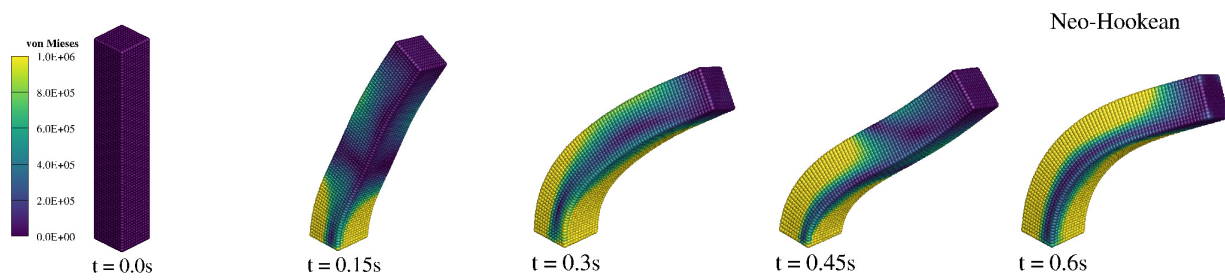
### 10.4. Mass diffusion

In this section, benchmark tests with available analytical solutions are investigated for validating the thermal and mass diffusion solvers in SPHinxsys.

The first test (folder "cases\_test/test\_2d\_diffusion") studied herein considers a 1D isotropic diffusion rectangle filled with water and a finite horizontal band of pollutant located in the middle of the rectangle. The initial conditions with both a constant and an exponential pollutant concentration distribution are considered. Figure 10.4a illustrates the comparison of the present predictions of the concentration distributions against the analytical solution. The second example considers an anisotropic diffusion process from a contaminant source in water, where the contaminant source is located in a two dimensional square computation domain and a higher anisotropic ratio is considered. Figure 10.4b shows the computational con-



(a) Oscillating beam



(b) Cantilever

Figure 10.2: SPHinXsys validations for the simulation of solid dynamics applications. (a) Particle and von Mises stress distributions in the deformed configuration with isotropic elastic model for 2D oscillating beam when the maximum deformation is reached. (b) Particle and von Mises stress distributions at different time instants in the deformed configuration with Holzapfel-Ogden model for a 3D bending cantilever.

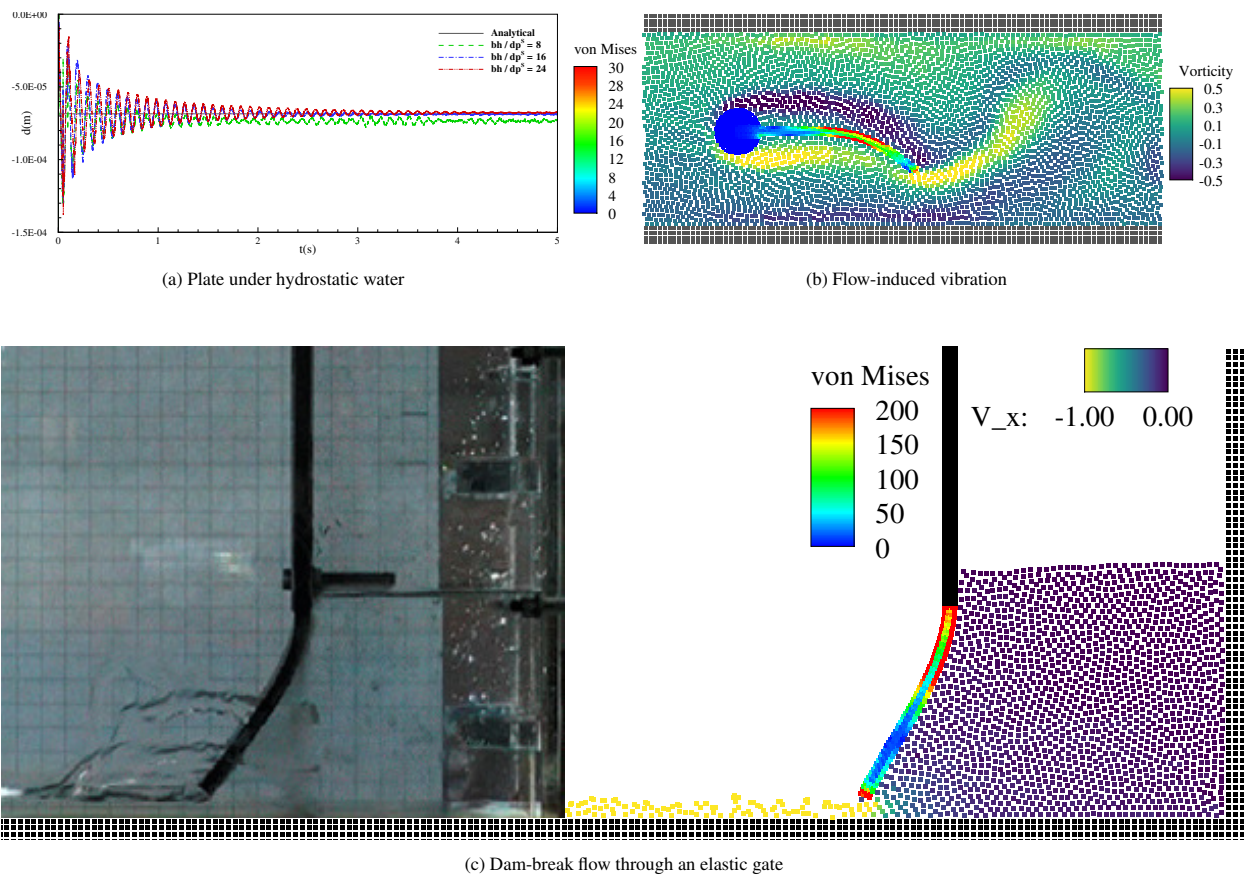


Figure 10.3: SPHinXsys validations and applications for FSI with a fluid-structure resolution ratio of 2. (a) The time history of mid-span displacement of an elastic plate under a hydrostatic water column. (b) The flow vorticity field and beam deformation of flow-induced vibration of a beam attached to a cylinder. (c) Snapshots for dam-break flow through an elastic gate compared against experimental frames [15].

centration distribution and the comparison with analytical solution. Figure 10.4c gives the numerical concentration distributions at horizontal cross section and vertical cross section and the corresponding analytical solution. It can be noted that SPHinXsys can accurately predict the concentration distribution in iso- and anisotropic diffusion processes.

### 10.5. Diffusion-reaction equation

In this part, SPHinXsys is validated for solving reaction-diffusion model by capturing the free-pulse propagation of transmembrane potential and reproducing the spiral wave in uniform and nonuniform computational domains.

The first benchmark test (folder "cases\_test/test\_2d\_depolarization") taken from Ratti and Verani [35] considers a transmembrane potential which propagates in a 2D isotropic tissue in a square domain. Figure 10.5a reports the predicted evolution profile of the transmembrane potential and the corresponding comparison with that of Ratti and Verani [35]. It is noted that in accordance with the previous numerical estimation and experimental observation, the quick propagation of the stimulus in the tissue and the slow decrease in the transmembrane potential after a plateau phase are well predicted. The second example considers the generation of an spiral wave in rectangular and circular geometries. Figure 10.5b and 10.5c show spiral waves of the stable rotation solution in rectangular and circular computational domain at different time instants. Also, both iso- and anisotropic diffusion coefficient tensors are taken into consideration. As expected, the spiral wave generates a curve and rotates clockwise as reported

### 10.6. Electromechanics

In this section, the validation of SPHinXsys in modeling electromechanics is presented and the application for biventricular heart model is also summarized.

To validate the electromechanics solver, we consider a benchmark (folder "cases\_test/test\_3d\_active\_myocardium") where a unit cube of myocardium with a linearly distributed transmembrane potential, whose time variation is neglected. The electro-mechanical coupling is governed by a ad-hoc activation law and the constitutive law describing the

passive response is the Holzapfel-Ogden model. Figure 10.6a shows the deformed configuration of the cubic myocardium and for the quantitative comparison with data in literature the reader is referred to Ref. [4]. In this application (folder "cases\_test/test\_3d\_electro\_mechanics"), the SPHinXsys is applied for modeling excitation-induced contraction of a generic biventricular heart model. Two cases with free-pulse and scroll wave propagation of the transmembrane potential are considered. Figure 10.6b shows the resulting excitation-contraction of the heart with the transmembrane potential contours.

## 11. Concluding remarks and future work

SPHinXsys v0.2.0 is an open source SPH research library featured by several numerical schemes dealing with: fluid dynamics, solid mechanics, thermal and mass diffusion, reaction diffusion, fluid-structure interaction, electromechanics and their coupling with rigid body dynamics. At present, the SPHinXsys major publications involve the validations and preliminary applications. SPHinXsys is developed and distributed on a GitHub public repository with comprehensive tutorials, thereby allowing the code availability and possible modification, along with the reproducibility of the published test cases.

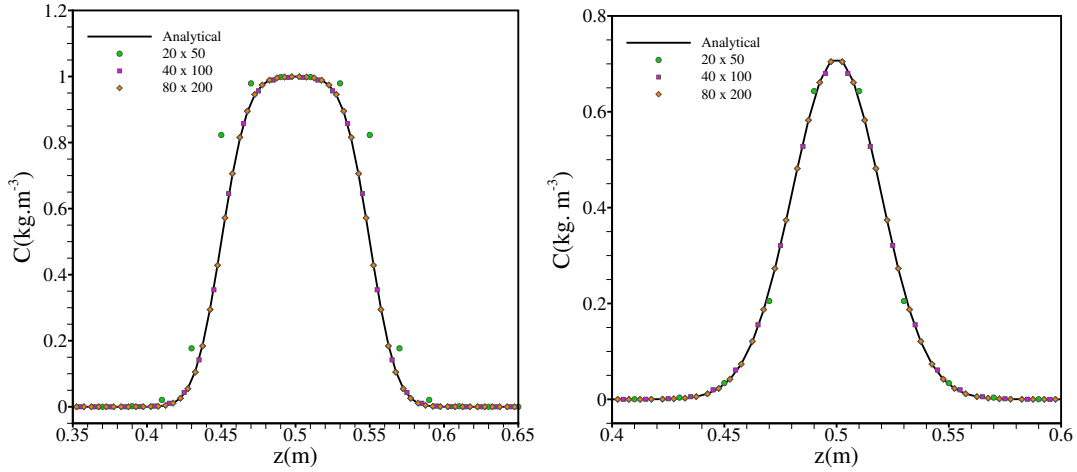
In the future, one improvement would be the optimization the computational efficiency by implementing graphics processing unit (GPU) accelerators combined with many-core parallelization strategy.

Another core aim is the development of an open heart simulator, which is expected to carry out numerical simulations of the total cardiac function [36], based on the SPH method.

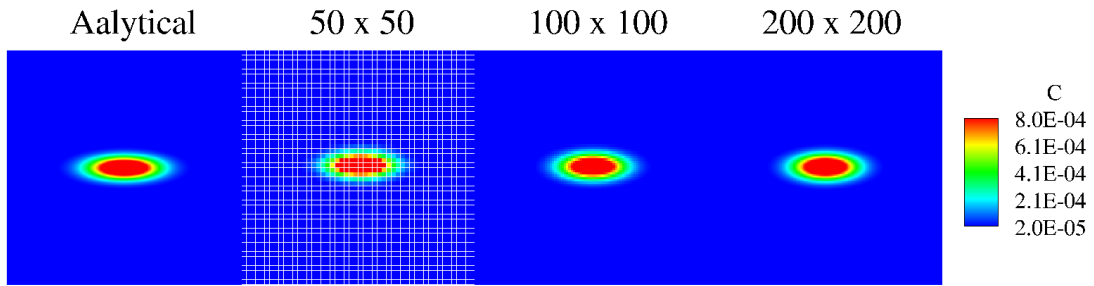
In addition, more industrial applications, e.g. oscillating wave energy converter (OWSC), will be added to the next version of SPHinXsys.

### CRediT authorship contribution statement

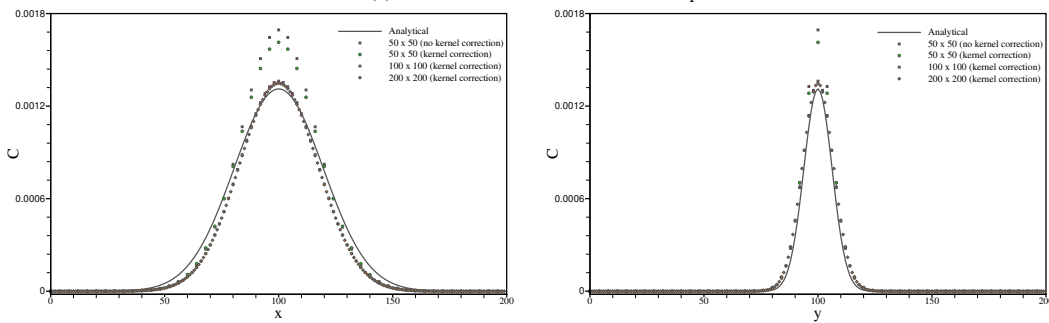
**Chi Zhang:** Conceptualization, Methodology, Software (coding and testing of existing library components), Validation, Formal analysis, Writing - original draft, Writing - review & editing, Visualization. **Massoud Reza-vand:** Methodology, Software (coding and testing of existing library components), Writing - review & editing.



(a) Isotropic diffusion with constant (left panel) and exponential (right panel) initial distributions.

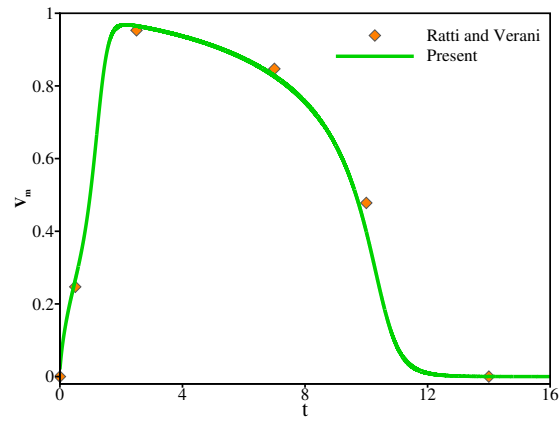


(b) Concentration distributions for anisotropic diffusion.

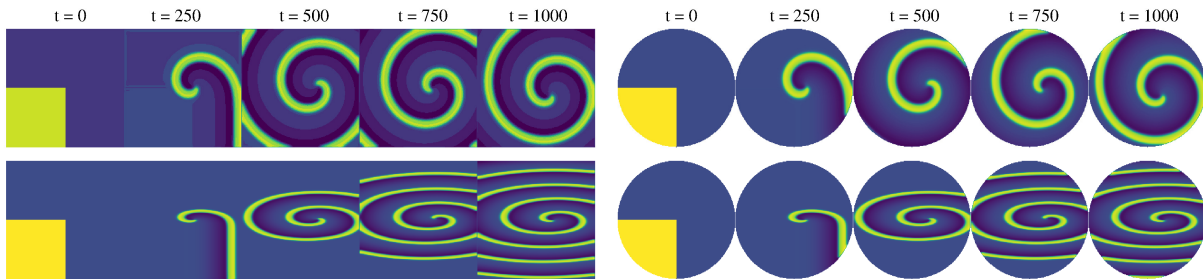


(c) Concentration distributions in x, and y-direction for anisotropic diffusion.

Figure 10.4: SPHinXsys validations for thermal diffusion with iso- and aniso-tropic diffusion tensor. (a) Concentration distribution for isotropic diffusion processes with constant and exponential initial concentration distributions. (b) Concentration distribution for anisotropic diffusion with anisotropic ratio equals 10. (c) Concentration distributions at horizontal cross in x, and y-direction for anisotropic diffusion.



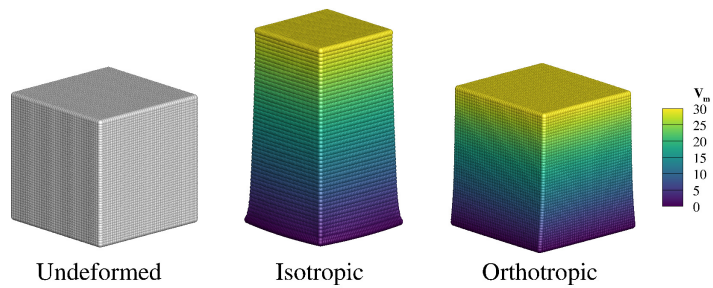
(a) Depolarization of transmembrane potential.



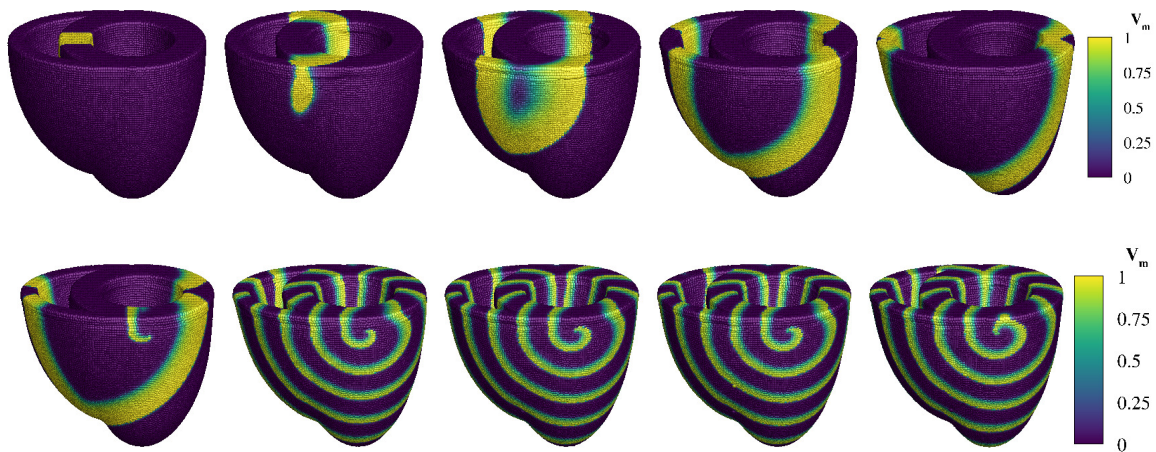
(b) Spiral wave in rectangular geometry.

(c) Spiral wave in circular geometry.

Figure 10.5: SPHinXsys validations and applications for reaction-diffusion equation (monodomain equation). (a) Time evolution of the transmembrane potential at point (0.3,0.7) in comparison with the results reported by Ratti and Verani [35]. (b) Spiral waves of the FitzHugh-Nagumo model in rectangular computational domain with iso- and anisotropic diffusion tensor. (c) Spiral waves of the FitzHugh-Nagumo model in circular computational domain with iso- and anisotropic diffusion tensor.



(a) Active response of cubic myocardium.



(b) Excitation-contraction of generic biventricular heart.

Figure 10.6: SPHinXsys validations and applications for electro-mechanical coupling. (b) Active response of the unit cubic myocardium with both isotropic and anisotropic material properties. (c) Generic biventricular heart: coupled excitation-contraction induced by the transmembrane potential as a free pulse (top panel) and scroll wave (bottom panel).

**Yujie Zhu:** Methodology, Software (coding and testing of existing library components), Writing - review & editing. **Yongchuan Yu:** Methodology, Software (coding and testing of existing library components). **Dong Wu:** Methodology, Software (coding and testing of existing library components). **Wenbin Zhang:** Methodology, Software (coding and testing of existing library components). **Jianhang Wang:** Methodology. **Xiangyu Hu:** Supervision, Conceptualization, Methodology, Software (coding and overview), Writing - review & editing .

### Declaration of competing interest

The authors declare that they have no known competing financial interests or personal relationships that could have appeared to influence the work reported in this paper.

### 12. Acknowledgement

The authors would like to express their gratitude to Deutsche Forschungsgemeinschaft for their sponsorship of this research under grant numbers DFG HU1527/10-1 and HU1527/12-1.

### References

### References

- [1] C. Zhang, X. Hu, N. A. Adams, A weakly compressible SPH method based on a low-dissipation riemann solver, *J. Comput. Phys.* 335 (2017) 605–620.
- [2] C. Zhang, M. Rezavand, X. Hu, Dual-criteria time stepping for weakly compressible smoothed particle hydrodynamics, *Journal of Computational Physics* 404 (2020) 109135.
- [3] C. Zhang, M. Rezavand, X. Hu, A multi-resolution sph method for fluid-structure interactions, arXiv preprint arXiv:1911.13255.
- [4] C. Zhang, J. Wang, M. Rezavand, D. Wu, X. Hu, An integrative smoothed particle hydrodynamics framework for modeling cardiac function, arXiv preprint arXiv:2009.03759.

- [5] L. B. Lucy, A numerical approach to the testing of the fission hypothesis, *The Astronomical Journal* 82 (1977) 1013–1024.
- [6] R. A. Gingold, J. J. Monaghan, Smoothed particle hydrodynamics: theory and application to non-spherical stars, *Mon. Not. R. Astron. Soc.* 181 (3) (1977) 375–389.
- [7] J. J. Monaghan, Simulating free surface flows with SPH, *J. Comput. Phys.* 110 (2) (1994) 399–406.
- [8] X. Hu, N. Adams, A multi-phase SPH method for macroscopic and mesoscopic flows, *J. Comput. Phys.* 213 (2006) 844–861.
- [9] S. Shao, C. Ji, D. I. Graham, D. E. Reeve, P. W. James, A. J. Chadwick, Simulation of wave overtopping by an incompressible SPH model, *Coastal Eng.* 53 (9) (2006) 723–735.
- [10] C. Zhang, G. Xiang, B. Wang, X. Hu, N. Adams, A weakly compressible SPH method with WENO reconstruction, *Journal of Computational Physics* 392 (2019) 1–18.
- [11] L. D. Libersky, A. G. Petschek, Smooth particle hydrodynamics with strength of materials, in: *Advances in the free-Lagrange method including contributions on adaptive gridding and the smooth particle hydrodynamics method*, Springer, 1991, pp. 248–257.
- [12] W. Benz, E. Asphaug, Simulations of brittle solids using smooth particle hydrodynamics, *Comput. Phys. Commun.* 87 (1) (1995) 253–265.
- [13] J. J. Monaghan, SPH without a tensile instability, *J. Comput. Phys.* 159 (2) (2000) 290–311.
- [14] P. Randles, L. Libersky, Smoothed particle hydrodynamics: some recent improvements and applications, *Comput. Methods Appl. Mech. Eng.* 139 (1-4) (1996) 375–408.
- [15] C. Antoci, M. Gallati, S. Sibilla, Numerical simulation of fluid–structure interaction by SPH, *Computers & Structures* 85 (11-14) (2007) 879–890.

- [16] L. Han, X. Hu, SPH modeling of fluid-structure interaction, *Journal of Hydrodynamics* 30 (1) (2018) 62–69.
- [17] M. Rezavand, C. Zhang, X. Hu, A weakly compressible sph method for violent multi-phase flows with high density ratio, *Journal of Computational Physics* 402 (2020) 109092.
- [18] J. P. Morris, P. J. Fox, Y. Zhu, Modeling low reynolds number incompressible flows using sph, *J. Comput. Phys.* 136 (1) (1997) 214–226.
- [19] S. Adami, X. Y. Hu, N. A. Adams, A transport-velocity formulation for smoothed particle hydrodynamics, *J. Comput. Phys.* 241 (2013) 292–307.
- [20] C. Zhang, X. Y. Hu, N. A. Adams, A generalized transport-velocity formulation for smoothed particle hydrodynamics, *J. Comput. Phys.* 337 (2017) 216–232.
- [21] S. Adami, X. Hu, N. Adams, A generalized wall boundary condition for smoothed particle hydrodynamics, *J. Comput. Phys.* 231 (21) (2012) 7057–7075.
- [22] G. A. Holzapfel, R. W. Ogden, Constitutive modelling of passive myocardium: a structurally based framework for material characterization, *Philosophical Transactions of the Royal Society of London A: Mathematical, Physical and Engineering Sciences* 367 (1902) (2009) 3445–3475.
- [23] R. Vignjevic, J. R. Reveles, J. Campbell, Sph in a total lagrangian formalism, *CMC-Tech Science Press* 4 (3) (2006) 181.
- [24] T. Tran-Duc, E. Bertevas, N. Phan-Thien, B. C. Khoo, Simulation of anisotropic diffusion processes in fluids with smoothed particle hydrodynamics, *International Journal for Numerical Methods in Fluids* 82 (11) (2016) 730–747.
- [25] R. FitzHugh, Impulses and physiological states in theoretical models of nerve membrane, *Biophys. J.* 1 (6) (1961) 445.
- [26] A. Quarteroni, A. Manzoni, C. Vergara, The cardiovascular system: mathematical modelling, numerical algorithms and clinical applications, *Acta Numerica* 26 (2017) 365–590.
- [27] R. R. Aliev, A. V. Panfilov, A simple two-variable model of cardiac excitation, *Chaos, Solitons & Fractals* 7 (3) (1996) 293–301.
- [28] A. Panfilov, Three-dimensional organization of electrical turbulence in the heart, *Physical Review E* 59 (6) (1999) R6251.
- [29] J.-H. Wang, S. Pan, X. Y. Hu, N. A. Adams, A split random time-stepping method for stiff and nonstiff detonation capturing, *Combustion and Flame* 204 (2019) 397–413.
- [30] K. Ten Tusscher, D. Noble, P.-J. Noble, A. V. Panfilov, A model for human ventricular tissue, *American Journal of Physiology-Heart and Circulatory Physiology* 286 (4) (2004) H1573–H1589.
- [31] M. P. Nash, A. V. Panfilov, Electromechanical model of excitable tissue to study reentrant cardiac arrhythmias, *Progress in biophysics and molecular biology* 85 (2-3) (2004) 501–522.
- [32] J. Wong, S. Göktepe, E. Kuhl, Computational modeling of electrochemical coupling: a novel finite element approach towards ionic models for cardiac electrophysiology, *Computer methods in applied mechanics and engineering* 200 (45-46) (2011) 3139–3158.
- [33] X. Yang, M. Liu, S. Peng, Smoothed particle hydrodynamics modeling of viscous liquid drop without tensile instability, *Computers & Fluids* 92 (2014) 199–208.
- [34] H. Wendland, Piecewise polynomial, positive definite and compactly supported radial functions of minimal degree, *Adv. Comput. Math.* 4 (1) (1995) 389–396.
- [35] L. Ratti, M. Verani, A posteriori error estimates for the monodomain model in cardiac electrophysiology, *Calcolo* 56. doi:10.1007/s10092-019-0327-2.

- [36] A. Quarteroni, T. Lassila, S. Rossi, R. Ruiz-Baier, Integrated heart—coupling multiscale and multi-physics models for the simulation of the cardiac function, *Computer Methods in Applied Mechanics and Engineering* 314 (2017) 345–407.